Nonlinear Dyn (2019) 98:2131–2145
https://doi.org/10.1007/s11071-019-05313-x

ORIGINAL PAPER

Modeling and dynamical analysis of a small-scale unmanned helicopter

Guoyuan Qi · **Donghui Huang**

Received: 12 January 2019 / Accepted: 21 October 2019 / Published online: 29 October 2019

Abstract A simple model comprising five differential equations reflecting the attitude dynamics of small-scale hovering helicopters is developed. From its force analysis, this helicopter system has the dynamic structure of a Kolmogorov model producing chaos. The stable-focus mode and chaotic mode are identified for the helicopter. The hidden chaotic attraction basin is identified, which demonstrates the multi-stability of the helicopter and highly sensitivity with initial location. Varying the configuration of the moment of inertia leads to a change in dynamics for the helicopter system. The analysis of its chaotic motion is significant for designing of the controller as well as the configuration of parameters so as to avoid instabilities that produce chaos through improper assembly or selection of materials. The Lyapunov exponent spectra and the two-parameter bifurcation in terms of moment of inertia exhibit rich dynamical modes: stable, periodic orbit, pseudo-periodic orbit, and chaotic. A perturbation feedback control method is applied to control the system subjecting to chaos situation to reach the periodic orbit or equilibrium point. This control just needs a single controller but does not need the control input computation. The proposed model and the discovery of chaos provide a benchmark for the design and research of control algorithms for similar helicopter systems.

Keywords Attitude dynamics · Small-scale unmanned helicopter · Chaos · Hidden chaotic attractor · Bifurcation · Control

G. Qi (✉)
Tianjin Key Laboratory of Advanced Technology of Electrical Engineering and Energy, School of Electrical Engineering and Automation, Tianjin Polytechnic University, Tianjin 300387, China
e-mail: guoyuanqisa@qq.com

D. Huang
School of Electrical Engineering and Automation, Tianjin Polytechnic University, Tianjin 300387, China
e-mail: huang152669@vip.qq.com

1 Introduction

With the advancement in communications and flight control technologies and composite materials, small-scale unmanned helicopters have broad applications such as in military surveillance, transmission line inspection, and environmental monitoring. Because of the highly nonlinear, open-loop instability and strong coupling among the axes, rotors, and flapping, the study of small-scale unmanned helicopter systems is very challenging [1,2]. The helicopter is generally a rigid body, so its dynamics complies with the Newton–Euler equation. When the helicopter is hovering, the dynamics obeys the generalized Euler equation. When the parameters are not configured well, the system may produce periodic oscillations, and even chaotic oscillation. Helicopters are highly nonlinear systems with significant dynamic coupling. This dynamic coupling is attributed to the interaction of inertial forces, gravitational forces, flipping forces, damping, torque, and moments generated by forces. There is also significant

parameter and modeling uncertainties because of the complicated aerodynamic nature of the thrust generation. Therefore, there is a major interest in the theoretical perspectives of helicopter controller designs and their flight dynamics.

The literature on flight control algorithms for helicopters is numerous, but may be divided into three categories: linear control, nonlinear control, and artificial intelligence control [3]. However, studies on the dynamics of small-scale unmanned helicopters based on a model are few, and the literature on chaotic dynamics has not been reported as best as we have ascertained.

To study the dynamics and chaos of such helicopters, building a simple and suitable model reflecting their dynamics is important. Current modeling divides the field mainly into first-principle modeling or mechanism modeling and system identification modeling [1]. The mechanism modeling approach requires significant knowledge about the helicopter flight dynamics in terms of, for example, flight mechanics, aerodynamics, rigid dynamics, and flipping angle dynamics [1,2,4]. The system identification modeling technique uses data obtained during flight tests to extract a simulation model. This approach is relatively simpler and does not require *a priori* knowledge of the system dynamics. The program, CIFER (Comprehensive Identification from Frequency Response), is typically used [5]. Most researchers combine both methods, in which the model structure and equations are developed using first principles and the parameters are identified using the identification approach [1,2,4,6,7].

Cai et al. [1] developed a model for the Raptor 90 including 6-DOF rigid body dynamics and main rotor flapping dynamics; the parameter values were evaluated using CIFER. However, the equations governing the source of force and moment and flipping dynamics are too complicated to analyze its dynamics. Bhandari and Colgren [4] modeled a full-sized version of the Raptor 50 using twelve differential equations including 6-DOF rigid body dynamics, flipping angle dynamics, and stabilizer dynamics. Koo and Sastry proposed a model with eight differential equations containing 6-DOF rigid body dynamics and two flipping angle dynamics. The model complexity is moderate and easy for analysis of the dynamics [2], and the model is the basis of many models of small-scale unmanned helicopters [6]. Pan et al. [7] developed a model using both first-principle methods and the PEM (Proton Exchange Membrane) identification method, which has quite a sophisticated design controller as well as dynamics analyzer. Mettler used CIFER to establish a linear state-space model of a hovering helicopter [8]. A neural network method was also used to identify the nonlinear model [9]. However, these complicated models are difficult to use and to base control algorithms and a dynamical analysis on. To study the dynamics and chaos of the small-scale helicopter, building a simple and suitable model reflecting its dynamics is necessary.

Most scholars focus on the control strategies and control performance using external forces to stabilize the closed-loop system. However, few scholars have studied the dynamics of open-loop systems before the design of the controller, including stability, oscillations, and the generation of different dynamical modes: sink, periodic orbit, pseudo-periodic orbit, chaos, and source. We find that by adjusting the values of some helicopter parameters or increasing the external disturbance, the angular momenta or velocities of the system may operate in a chaotic behavior.

The presence of chaos in the helicopter dynamics physically causes the system to oscillate and to create acoustic noise and mechanical vibration, thereby consuming electrical energy and reducing service life. If we control it with force to stabilize the system, the strong control forces will damage the actuators. The best way is to design the helicopter to avoid parameter configurations that generate chaos. In addition, to design a suitable controller for a small helicopter, the first task is to study its dynamics to know the possible behavior prior to or during the control operation. Therefore, building a simulation model of a helicopter and studying its chaotic dynamics are paramount in both scientific research on chaos and practical applications. Analyzing physical systems from the perspective of chaos applies not only in helicopter design to avoid chaos, but also in the design of large passenger aircraft in adapting to aerodynamic conditions, wind turbine power generation, and small satellites.

Why is there a lack of chaos research of small-scale helicopters? One reason is that, usually, the Euler angles, spatial positions, and speed of a closed-loop system are measured and evaluated, instead of angular velocity or angular momentum, and the latter are often present in chaotic modes for a rigid body according to research [10–13]. The generalized Euler equation, or often-called Kolmogorov model describing a forced rigid body, has cross-quadratic terms, linear terms, dissipative terms, and external force terms. From this point

of view, an analogy between this dissipative chaotic system and a forced rigid body is made [10–13]. In addition, the angular momenta or angular velocities of a rigid body are analogous to the states of a dissipative chaotic system. Another reason for the scarcity is that most scholars focus on the control performance using external forces for the closed-loop system, whereas the dynamics of an open-loop system have not been studied as much.

Many mathematical chaotic systems have been constructed. These systems are basically based on other existing chaotic systems, such as the Lorenz chaotic system or the Chua chaotic circuit system, to obtain a series of new chaotic systems, the hyperchaotic systems, or chaotic systems with memoristor, by tentatively increasing the importance of linear or nonlinear terms or the dimensions of the system. However, these systems have been developed mathematically. A few chaotic models or systems have been derived from practical engineering scrutiny or observations of physical processes, such as the brushless DC motor chaotic system [10,11,14], the plasma chaotic system [15–17], a 4D rigid body conservative chaotic system [18], and the nuclear spin generator system [19]. Those systems derived from a physical process are called physical chaotic systems to distinguish them from mathematical chaotic systems.

This paper develops a simple dynamical model for the hovering with five differential equations reflecting the attitude dynamics of the small-scale unmanned helicopter. The stabilizer dynamics and fuselage force are reasonably neglected. An analysis of the dynamics is performed. The stable-focus mode, periodic orbits, pseudo-periodic orbital mode, and chaotic mode are identified and analyzed. The basic mechanism that produces chaos is studied using force analysis. The hidden chaotic attractor is identified, which demonstrates the multi-stability of the helicopter and highly sensitivity with initial location. Bifurcations with respect to the moments of inertia of the helicopter are provided. The emergence of chaos that may cause damage and how to prevent it in helicopter maneuverings is pointed out. Finally, a single-channel controller for the MIMO system is designed using the method proposed by Tereshko in [20]. The paper is organized as follows:

Section 2 describes the dynamical model of small-scale helicopter, which comprises five differential equations. Section 3 analyzes the dynamics of equilibrium points and the hidden chaotic attractor. A bifurcation analysis is performed in Sect. 4. Section 5 presents conclusions. A perturbation control method is adopted to effectively control the chaotic system. For brevity, the term helicopter from here on shall refer specifically to a small-scale unmanned helicopter unless otherwise stated.

2 Dynamical model of the helicopter

To date, the modeling of a helicopter has seen some progress particularly when the system identification and mechanism modeling methods are combined. We develop a nonlinear model along these lines by simplifying the work in [1,2,6,21]. This paper only studies the dynamics associated with hovering. Only two coordinate frames need to be considered: the body coordinate frame and the local north-east-down (NED) coordinate frame. Actually, a body in flight needs the vehicle-carried NED coordinate frame to describe the motion. However, when the helicopter moves only within a small region at low speed, especially when we study the attitude dynamics of hovering, it is reasonable to assume that the direction of the vehicle-carried and local NED coordinate systems constantly coincides with each other. The origin of the body coordinate frame is located at the center of mass of the helicopter. The x axis points to the front of the body, the y axis points to the right side of the body, and the z axis points downward complying with the right-hand rule of vector products. The local NED coordinate frame and the body coordinate frame are demonstrated as Fig. 1. The body frame rotates, and Local NED is fixed. The relationship between the two frames is described by the rotational matrix in Eq. (4).

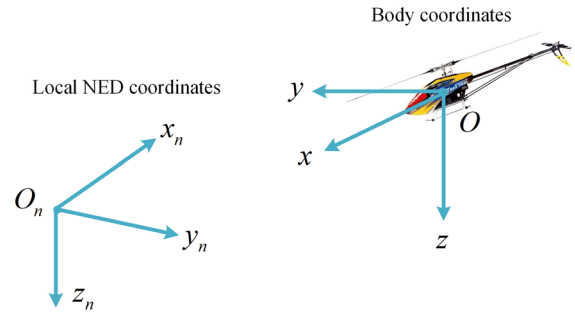

Fig. 1 Schemes of local NED coordinate frame and the body coordinate frame

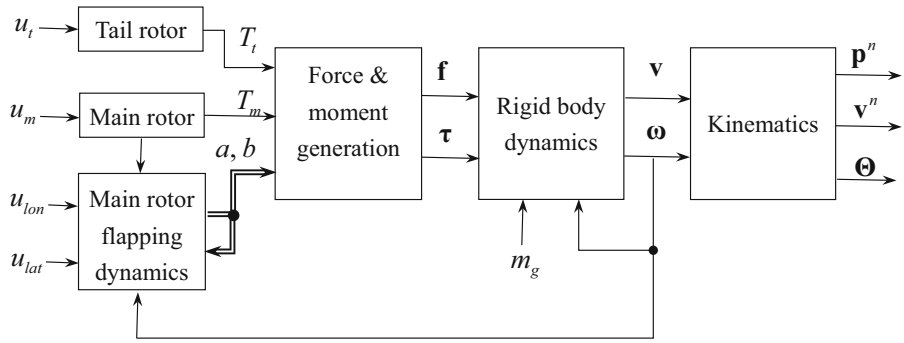

Fig. 2 Helicopter dynamics

A helicopter model can be divided into four parts: (1) the power sources, (2) the force and moment generation process, (3) the rigid body dynamics, and (4) the kinematics (Fig. 2). The power sources include the main rotor and tail rotor. Both thrusts are subjected to control inputs, fuselage, vertical fin, and horizontal fin. The flapping angles are outputs of the main rotor flapping dynamics and used in adjusting the tip path-flapping blades, which directly determine the rigid body dynamics. The generation of forces and moments accounts for several of the algebraic equations. The model of the rigid body dynamics includes the Newton–Euler equation, which produce the body velocity and angular velocity given the force and moment exerted on center of the flight body, and the kinematics contain the dynamical equation associated with the transformation between the body coordinate and inertial frames.

We present the rigid body dynamics, kinematics, and the dynamics of the flapping angles of the main rotor following the work in References [1,2,6,21].

2.1 Dynamics of a rigid body

If the helicopter is regarded as a rigid body, its dynamics model involves two aspects: translational motion and, in regard to attitude, rotational motion. In being subjected to body force $\mathbf{f} \in R^3$ and torque $\boldsymbol{\tau} \in R^3$ in the body coordinate frame applied at the center of gravity (CG), the dynamics of this rigid body is given by the Newton–Euler equation for the translational motion,

$$m\dot{\mathbf{v}} = m\mathbf{v} \times \boldsymbol{\omega} + \mathbf{f}, \tag{1}$$

and for the rotational motion,

$$\mathbf{I}\dot{\boldsymbol{\omega}} = \mathbf{I}\boldsymbol{\omega} \times \boldsymbol{\omega} + \boldsymbol{\tau}, \tag{2}$$

where $\mathbf{v} = \left[v_x,\ v_y,\ v_z\right]^{\mathrm{T}} \in R^3$ is the body velocity, $\boldsymbol{\omega} = \left[\omega_x,\ \omega_y,\ \omega_z\right]^{\mathrm{T}} \in R^3$ the body angular velocity, $m \in R^1$ the mass, and $\mathbf{I} = diag\,(I_1,\ I_2,\ I_3)$ the principle inertial matrix.

2.2 Kinematics

The kinematics of the helicopter system is concerned with its translational and rotational motions and the dynamical transformation between local NED, which is assumed to be inertial, and the body coordinate frames. For the translational motion, we have

$$\dot{\mathbf{p}}^n = \mathbf{v}^n = R(\boldsymbol{\Theta})\mathbf{v}, \tag{3}$$

where $R(\boldsymbol{\Theta})$ is the rotational matrix from the body frame to the NED frame and is given by

$$R(\boldsymbol{\Theta}) = \begin{bmatrix} \mathrm{c}\theta\mathrm{c}\psi & \mathrm{s}\phi\mathrm{s}\theta\mathrm{c}\psi - \mathrm{c}\phi\mathrm{s}\psi & \mathrm{c}\phi\mathrm{s}\theta\mathrm{c}\psi + \mathrm{s}\theta\mathrm{s}\psi \\ \mathrm{c}\theta\mathrm{s}\psi & \mathrm{s}\phi\mathrm{s}\theta s\psi + \mathrm{c}\phi\mathrm{c}\psi & \mathrm{c}\phi\mathrm{s}\theta\mathrm{s}\psi - \mathrm{s}\phi\mathrm{c}\psi \\ -\mathrm{s}\theta & \mathrm{s}\phi\mathrm{c}\theta & \mathrm{c}\phi\mathrm{c}\theta \end{bmatrix} \tag{4}$$

with $\mathrm{s}* = \sin(*)$ and $\mathrm{c}* = \cos(*)$, $\boldsymbol{\Theta} = \left[\phi\ \theta\ \psi\right]^{\mathrm{T}}$. $R(\boldsymbol{\Theta})$ is given by the ZYX Euler angles denoted ϕ, θ, and ψ about the x, y and z axes, respectively. The rotational motion is given by

$$\begin{aligned} \dot{\boldsymbol{\Theta}} &= \Psi(\boldsymbol{\Theta})\boldsymbol{\omega} \\ &= \begin{bmatrix} 1 & \mathrm{s}\phi\mathrm{t}\theta & \mathrm{c}\phi\mathrm{t}\theta \\ 0 & \mathrm{c}\phi & -\mathrm{s}\phi \\ 0 & \mathrm{s}\phi/\mathrm{c}\theta & \mathrm{c}\phi/\mathrm{c}\theta \end{bmatrix} \boldsymbol{\omega} \end{aligned} \tag{5}$$

with $\mathrm{t}* = \tan(*)$.

2.3 Force and moment

As well as a horizontal stabilizer, a vertical stabilizer, and fuselage, a helicopter system comprises a lumped power source consisting of a main rotor producing thrust T_m and a tail rotor producing thrust T_t. Assuming the helicopter is operating at low speed, hence the

drag from the stabilizers and fuselage can be ignored in accounting for the power sources, as is adopted in [2,6]. Therefore, the external force exerting on the system is

$$\begin{aligned}\mathbf{f} &= \mathbf{f}_m + \mathbf{f}_t + \mathbf{f}_{mg} \\ &= \begin{bmatrix} x_m \\ y_m \\ z_m \end{bmatrix} + \begin{bmatrix} 0 \\ y_t \\ 0 \end{bmatrix} + R^{\mathrm{T}}(\boldsymbol{\Theta}) \begin{bmatrix} 0 \\ 0 \\ mg \end{bmatrix}, \end{aligned} \tag{6}$$

where $\mathbf{f}_m$ and $\mathbf{f}_t$ are the respective forces generated by the thrusts of the main rotor and tail rotor, and $\mathbf{f}_{mg}$ is the gravitational force, $R^{\mathrm{T}}(\boldsymbol{\Theta})$ rotates the gravitational force from the NED frame to the body coordinate frame. In detail, the forces are written

$$\begin{aligned} &x_m = -T_m sa,\ \ y_m = T_m sb,\ \ z_m = -T_M cacb, \\ &y_t = -T_t. \end{aligned} \tag{7}$$

where a and b are the flapping angles of the main rotor blades. Note that the thrust of the tail rotor is regarded as a source of lateral force y_t satisfying $y_t = -T_t$.

Similarly, the total torque is

$$\begin{aligned}\boldsymbol{\tau} &= \boldsymbol{\tau}_m + \boldsymbol{\tau}_t + \mathbf{m}_m + \mathbf{m}_t \\ &= \begin{bmatrix} K_\beta sb - Q_m sacb \\ K_\beta sa + Q_m sbca \\ -Q_m cacb \end{bmatrix} + \begin{bmatrix} 0 \\ -Q_t \\ 0 \end{bmatrix} \\ &\quad + \begin{bmatrix} y_m h_m \\ -x_m h_m \\ 0 \end{bmatrix} + \begin{bmatrix} y_t h_t \\ 0 \\ -y_t l_t \end{bmatrix}, \end{aligned} \tag{8}$$

where $\boldsymbol{\tau}_m$ and $\boldsymbol{\tau}_t$ denote the torques generated by the main rotor and tail rotor, respectively, and $\mathbf{m}_m$ and $\mathbf{m}_t$ the moments generated by the forces $\mathbf{f}_m$ and $\mathbf{f}_t$; K_β is the spring constant of the main rotor, h_m and h_t are the main hub locations of the main rotor and tail rotor above the CG of the helicopter system; l_t is the tail rotor hub location behind the system's CG; and Q_m and Q_t are air resistance torques with [6,21]

$$Q_m \simeq C_m T_m^{1.5} + D_m,\ \ Q_t \simeq C_t T_t^{1.5} + D_t. \tag{9}$$

The thrusts of main rotor and tail rotor are obtained from

$$T_m = K_m u_m + B_m,\ T_t = K_t u_t + B_t, \tag{10}$$

where u_m and u_t represent control inputs of the main rotor and tail rotor, and K_m, K_t, B_m, B_t are obtained by system identification using experimental data [1].

2.4 Main rotor flapping dynamics

Apart from the main thrust and tail thrust, the other important source of forces and torques is determined by the flapping angles a and b which are the longitudinal and lateral tilts in the tip path plane of the main rotor with respect to the shaft. The dynamics associated with the main rotor flapping angles is represented by two coupled first-order differential equations [2,21],

$$\begin{aligned} \dot{a} &= -\omega_y - 1/\tau a + A_b b + A_{lon} u_{lon}, \\ \dot{b} &= -\omega_x - 1/\tau b + B_a a + A_{lat} u_{lat}. \end{aligned} \tag{11}$$

where A_b and B_a represent the coupling strength between longitudinal and lateral flapping motions, respectively; A_{lon} and A_{lat} the coefficients of the cyclic control inputs u_{lon} and u_{lat}.

2.5 General model of the helicopter's altitude

Because we assume the helicopter is in hovering mode, only the rotational motion is actively operating. Therefore, the dynamic model of system combines Eqs. (2), (7), (8), and (11), which are written as five differential equations:

$$\begin{aligned} I_x \dot{\omega}_x &= (I_y - I_z)\omega_y \omega_z + (K_\beta + h_m T_m) sb \\ &\quad - Q_m sacb - h_t T_t, \\ I_y \dot{\omega}_y &= (I_z - I_x)\omega_x \omega_z + (K_\beta + h_m T_m) sa \\ &\quad + Q_m sbca - Q_t, \\ I_z \dot{\omega}_z &= (I_x - I_y)\omega_x \omega_y - Q_m cacb + l_t T_t, \\ \dot{a} &= -\omega_y - 1/\tau a + A_b b, \\ \dot{b} &= -\omega_x - 1/\tau b + B_a a. \end{aligned} \tag{12}$$

Some values of the parameters follow those given in [6,21], which were determined for MIT's small-scale rotorcraft X-Cell 60. All the parameter values are listed in Table 1. To maintain the helicopter in a hovering position, we take

$$T_m = mg,\ \ T_t = Q_m / l_t,\ \ u_{lon} = u_{lat} = 0., \tag{13}$$

where the setting $T_m = mg$ counteracts the gravitational force. Note that terms $A_{lon} u_{lon}$ and $B_{lat} u_{lat}$ vanish in Eq. (12) because $u_{lon} = u_{lat} = 0$.

3 Dynamical analysis of a hovering helicopter

The whole dynamics of the helicopter's attitude while hovering is governed by Eq. (12), from which we obtain the angular velocities of the body, ω_x, ω_y, ω_z and the flapping angles a and b. From Eq. (5), we solve for the Euler angles ϕ, θ, and ψ by combining it with Eq. (12).

Table 1 Parameter settings of the small-size unmanned helicopter

Parameter	Value	Parameter	Value
m	8.2 kg	K_β	52 N m/rad
g	9.78 m/s^2	B_{lat}	4.2
I_x	0.18 kg m^2	A_{lon}	4.2
I_y	0.34 kg m^2	A_b	3.629 s^{-1}
I_z	0.28 kg m^2	B_a	3.993 s^{-1}
h_m	−0.235 m	τ	0.1 s^{-1}
h_t	0.08 m	K_m	80.44
l_t	0.91 m	C_m	0.004452 m/$\sqrt{N}$
C_t	0.005066 m/$\sqrt{N}$	D_m	0.6304 N m
D_t	0.008488 N m	B_m	88.48
K_t	18.46	B_t	4.22

3.1 Simple force analysis

System (12) is a highly nonlinear coupled system. The vector form of the first three equations in Eq. (12) is displayed in Eq. (2). The term $\mathbf{I}\omega \times \boldsymbol{\omega}$ is the inertial part and produces nonlinear skew-symmetric quadratic terms. The torque term, $\boldsymbol{\tau}$, decomposes into four terms

$$\begin{aligned}\boldsymbol{\tau} &= \boldsymbol{\tau}_m + \boldsymbol{\tau}_t + \mathbf{m}_m + \mathbf{m}_t \\ &= \begin{bmatrix} K_\beta sb - Q_m sacb \\ K_\beta sa + Q_m sbca \\ -Q_m cacb \end{bmatrix} + \begin{bmatrix} 0 \\ -Q_t \\ 0 \end{bmatrix} + \begin{bmatrix} y_m h_m \\ -x_m h_m \\ 0 \end{bmatrix} \\ &\quad + \begin{bmatrix} y_t h_t \\ 0 \\ -y_t l_t \end{bmatrix}.\end{aligned}$$

Therefore, the torque exerted on the hovering body is a strongly coupled combination of torques generated by the main rotor and tail rotor and associated moments. In addition, there is a coupling of the rotational dynamics and flipping dynamics through the main rotor torque and the flipping angles that involve trigonometric functions. Two types of torque are generally in play; one is the applied torque or external torque, which acts to move the hovering body, and the another a dampening torque such as the terms involving Q_m and Q_t, which are related to air resistance, and damping terms $-1/\tau a$ and $-1/\tau b$ in the fourth and fifth equations in Eq. (12), respectively. Both the applied and dissipative torques are coupled, and therefore, the helicopter system is a strong nonlinear system.

The system is dissipative, because

$$\nabla \cdot V = \frac{\partial \dot{\omega}_x}{\partial \omega_x} + \frac{\partial \dot{\omega}_y}{\partial \omega_y} + \frac{\partial \dot{\omega}_z}{\partial \omega_z} + \frac{\partial \dot{a}}{\partial a} + \frac{\partial \dot{b}}{\partial b} = -\frac{2}{\tau} < 0. \tag{14}$$

Remark 1 The system model is a generalized Euler equation or Kolmogorov model [12], containing quadratic inertial torques, dissipative torques, and an external torque.

Given a Kolmogorov model with the forces or torques is coupled together, the trajectories of the system are twisted. There arises the possibility that energy exchange is irregular between the supplied energy provided by external torque and the absorbed energy lost through dissipative torque. From an analysis of the Qi chaotic system [13], the Qi four-wing chaotic system [12], the Chen system [22], the brushless DC motor chaotic system [11], and plasma chaotic system [16,17], we conclude that the Kolmogorov model contains a dynamical structure to produce chaos.

Remark 2 The helicopter system has a similar dynamical structure to the Kolmogorov model from which chaos emerges.

An analysis detailing the forces and energy exchanges required to reveal the mechanism underlying chaos generation is not studied in this paper. A study of this rich topic is left as an open problem for readers. In the following sections, we focus on the dynamical analysis.

3.2 Dynamics of equilibrium point when $I_x = 0.18$ kg m^2, $I_y = 0.34$ kg m^2, I_z=0.28 kg m^2

All parameter settings will be those listed in Table 1. We take $T_t = 4$N to keep the helicopter from rotating around the z axis.

With the appearance of trigonometric functions, there is an infinite number of equilibria, and it is quite difficulty to solve for the equilibria. We obtain two equilibrium points E_1 and E_2 for the given parameter settings (Table 1),

$$\begin{aligned} E_1 &= \left[\omega_x,\ \omega_y,\ \omega_z,\ a,\ b\right]^{\mathrm{T}}_{E_1} = [-0.9401,\ 1.1036, \\ &\quad -29.5451, -0.0892, 0.0584]^{\mathrm{T}}, \\ E_2 &= \left[\omega_x,\ \omega_y,\ \omega_z,\ a,\ b\right]^{\mathrm{T}}_{E_2} = [-54.23505, \\ &\quad -0.73977,\ 4.12451,\ 2.3882,\ 6.37712]^{\mathrm{T}}, \end{aligned}$$

With a sampling time of 0.001s in simulations, all values were initialized to zero, which is within the neighborhood of E_1. We make the following observations. The angular velocities ω_x and ω_y of the hovering body start from zero, and approach approximate steady states with quite small values of $\omega_x \approx -0.9401$(rad/s) and $\omega_y \approx 1.1036$ (rad/s) (Fig. 3a), which means that the hovering body remains almost stationary in the $x-y$ plane during the whole process. However, the angular velocity ω_z approaches a large value of $\omega_z \approx -29.5451$ (rad/s) (Fig. 3a). The reason is that the body is subjected to a tail rotor torque of $T_t = 4$N; specifically, from a top view, it turns clockwise at constant speed. Figure 3b gives the Euler angles during time interval $t \in [50,\ 60]$s where the roll angle, ϕ, and pitch angle, θ, periodically oscillate within quite small amplitudes, while the yaw angle, ψ, increases constantly, matching the spin of the body around the z axis. Clearly, the body is hovering and operates normally under open-loop control. Note that the constant velocities ω_x and ω_y do not mean the Euler angles, and ϕ and θ increase constantly; rather, they move periodically within small amplitudes, because the Euler angles are not simply the integrals of angular velocities, but included are kinematics described by Eq. (5).

The Jacobian matrix of any equilibrium of the hovering system is

$$J = \begin{bmatrix} 0 & (I_y - I_z)/I_x\omega_z & (I_y - I_z)/I_x\omega_y & -Q_m cacb/I_x & \big((K_\beta + h_m T_m)cb + Q_m sasb\big)/I_x \\ (I_z - I_x)/I_y\omega_z & 0 & (I_z - I_x)/I_y\omega_x & \big((K_\beta + h_m T_m)ca - Q_m sasb\big)/I_y & -Q_m cacb/I_y \\ (I_x - I_y)/I_z\omega_y & (I_x - I_y)/I_z\omega_x & 0 & Q_m sacb/I_z & Q_m casb/I_z \\ 0 & -1 & 0 & -1/\tau & A_b \\ -1 & 0 & 0 & B_a & -1/\tau \end{bmatrix} \tag{15}$$

The eigenvalues for equilibrium E_1 are

$$\lambda_{1,2} = -7.4085 \pm j11.8610,\ \lambda_3 = -2.5928,\ \lambda_{4,5} = -1.2951 \pm j0.7055.$$

Therefore, the equilibrium point is a sink or a stable focus because all real parts of the eigenvalues are negative. The maximum Lyapunov exponent (LE) is $L_1 = -1.2304$ for the given initial values at the origin, which matches observations (Fig. 3a). The trajectories start from the origin within the neighborhood of the equilibrium and converge to a fixed point. Note that the sink represents the stability of Eq. (12) and not of Eq. (5). In another words, the angular velocities $\boldsymbol{\omega} = \left[\omega_x,\ \omega_y,\ \omega_z\right]^{\mathrm{T}}$ converge to steady states (Fig. 3a), whereas the Euler angles $\boldsymbol{\Theta} = \left[\phi\ \theta\ \psi\right]^{\mathrm{T}}$ do not (Fig. 3b). The eigenvalues of E_2 are

$$\lambda_{1,2} = 0.5462 \pm j20.7413,\ \lambda_3 = 12.0954,$$
$$\lambda_{4,5} = -4.4984 \pm j12.4373.$$

Therefore, the equilibrium point is a saddle-focus point. Is it possible that the hovering body produces chaos when we initialize the system in the neighborhood of E_2? From Remark 2, the torque of the hovering body contains inertial, dissipative, and external torques, making chaos possible. Here, we examine the possibility by initializing $\omega_{x0} = -54, \omega_{y0} = -0.7,\ \omega_{z0} = 4,\ a = 2,\ b = 6$; the angular velocities oscillate considerably and irregularly within a large amplitude (Fig. 3c). The flipping angles also evolve abnormally (Fig. 3d). Figure 3e shows that a chaotic attractor exists in the 3D spatial view. The maximum LE is $L_1 = 1.10866$ for the given initialization (Fig. 3f) and confirms that the hovering helicopter operates in chaotic mode.

3.3 Hidden chaotic attractors

There are several types of hidden chaotic attractors. For one type, the basin of chaotic attraction does not intersect with small neighborhoods of the unstable fixed point [23,24], i.e., the basins of attraction of these attractors do not touch unstable fixed points and are located far away from such points. In another type, the attractor exists in the system without any equilibrium point or with the stable equilibrium point. In a third type, the attractor exists in infinitely many unstable equilibria.

The hovering helicopter system has many hidden chaotic attraction sets. For the settings given in Table 1, around the stable equilibrium point, E_1, the sink modes produce a large attractive basin starting from which the trajectories approach E_1 (Fig. 4). To determine the attractive basin in terms of variables ω_x and ω_y, we fix the values of ω_z, a, and b at equilibrium point E_1. The stable equilibrium point is marked with a white star (Fig. 4a). The blue region is the sink attractive basin and red region is the chaotic attractive basin in

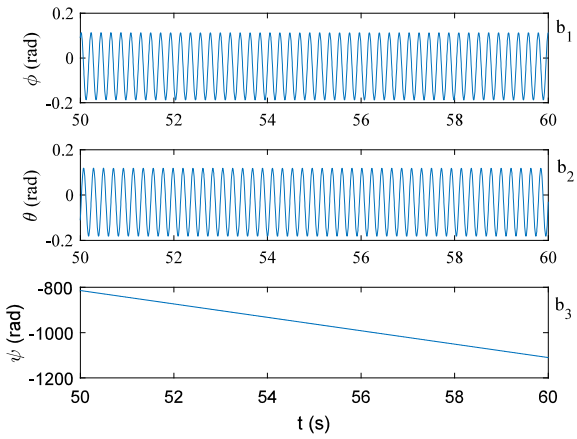

(a) Time response of ω_x, ω_y, and ω_z

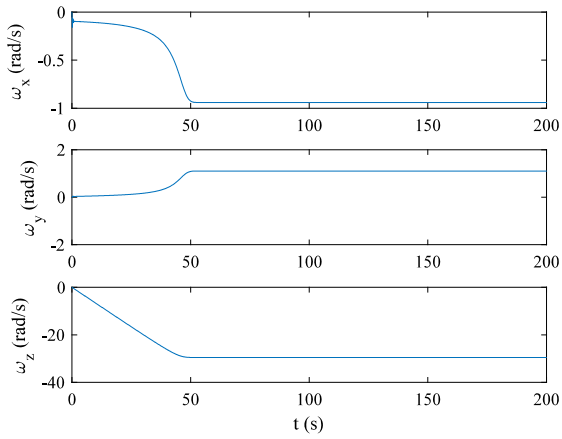

(b) Time response of Euler angles ϕ, θ, and ψ

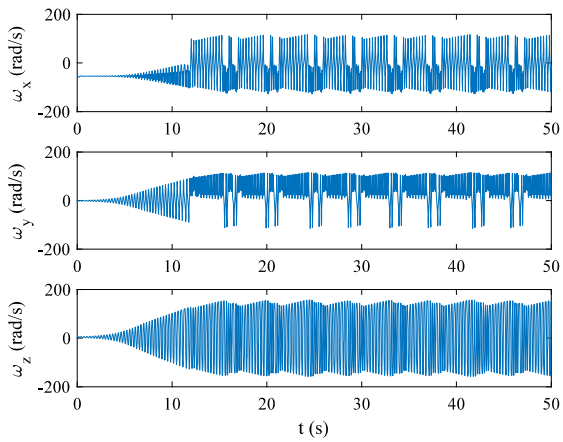

(c) Time response of ω_x, ω_y and ω_z

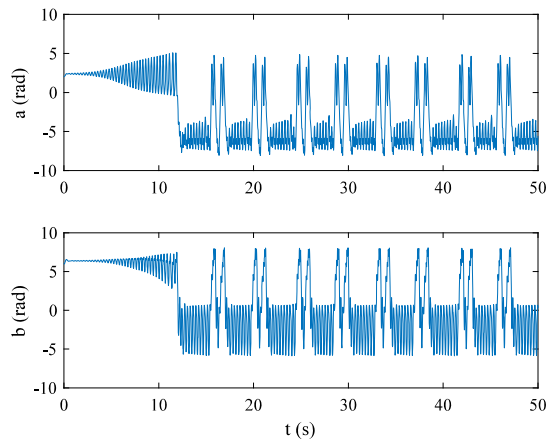

(d) Time response of flipping angles a and b

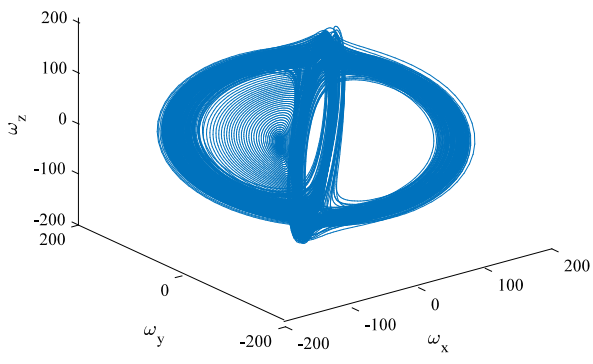

(e) 3D spatial view

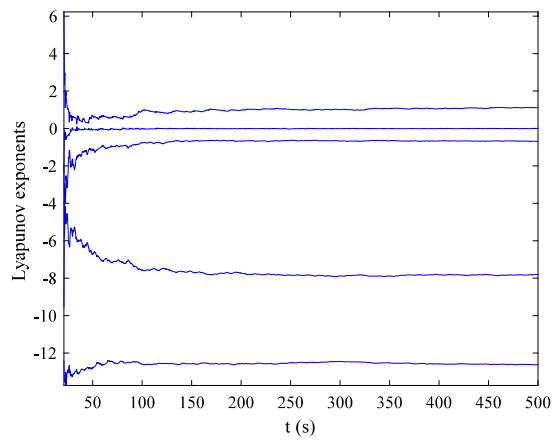

(f) Lypunov exponents

Fig. 3 Sink modes and chaotic modes with moment of inertia $I_x = 0.18\ \mathrm{kg\,m^2}$, $I_y = 0.34\ \mathrm{kg\,m^2}$, I_z=0.28 $\mathrm{kg\,m^2}$, where **a**, **b** initial values being at the origin, and **c**–**f** at $[-54,\ -0.7,\ 4,\ 2,\ 6]^{\mathrm{T}}$.

which the hidden chaotic attractors are produced. To establish clearly the hidden attraction basin, we plotted three trajectories, each starting from different locations (Fig. 4a). In Fig. 4b, the blue trajectory starts at point $[35,\ 35,\ -29.5451]^{\mathrm{T}}$, which belongs to the sink basin in Fig. 4a. The starting point is marked with a blue solid point. The spiral trajectory oscillates for a short while and then converges to the sink, E_1, marked by a black star. The black trajectory starts at point $[-20,\ 0,\ -29.5451]^{\mathrm{T}}$, also belonging to the sink basin, and spirals rapidly to E_1. The third trajectory is a chaotic curve starting at point $[60,\ 0,\ -29.5451]^{\mathrm{T}}$ belonging to the chaotic attraction basin. The chaotic trajectory oscillates irregularly with large amplitudes and runs around the periphery of the sink basin.

3.4 Dynamics of the equilibrium point when $I_x = 0.29\mathrm{kg\,m^2}$, $I_y = 0.233\mathrm{kg\,m^2}$, $I_z = 0.236\mathrm{kg\,m^2}$

Variations in configuration of the moment of inertia leads to changes in dynamics of the hovering helicopter. For instance, we set $I_x = 0.29\mathrm{kg\,m^2}$, $I_y = 0.233\mathrm{kg\,m^2}$, $I_z = 0.236\mathrm{kg\,m^2}$, while all other parameters in Table 1 remain the same. We took initial values at the origin as starting points (Fig. 4). However, the helicopter leaves the stable-focus mode after a period of time and enters into a chaotic mode (Fig. 5a). The angular velocities ω_x and ω_y of the helicopter stay at zeros for about 165 s and then suddenly enters a chaotic mode, oscillating significantly and irregularly, while ω_z decreases constantly and then enters a chaotic mode as well. The system produces a chaotic attractor (Fig. 5b) with a maximum LE of $L_1 = 3.992$.

We offer an explanation of why the chaos for the helicopter system has not been reported previously. Normally, scholars and engineers pay more attention on control, so open-loop controlled hovering had not been given much attention. Moreover, researchers focus on the changes in Euler angles, positions, and translational velocities rather than angular velocities. However, we have taken the latter into account explicitly in Eq. (12). When we only tested the Euler angles using Eq. (5), we did not observe chaotic modes (Fig. 5c). The roll angle remains steady around zero up to 165 s, but then suddenly decreases thereafter when the angular velocities exhibit chaos. However, the roll angle exhibits no chaos; the body instead spirals, i.e., rolls around the x axis in a clockwise direction. The pitch angle oscillates within a small range and does not exhibit chaos either. The yaw angle decreases continuously from the beginning, which means the helicopter rotates constantly around the z axis because of the action of the torque of the tail rotor, $T_t = 4$. To show clearly the pitch angle, we have only plotted it in the time interval $[195,\ 200]$, otherwise its trajectory would be too dense to observe.

Remark 3 The dynamics of a helicopter system are complicated featuring various modes in different regions of parameter space and different parametric configurations.

Remark 4 The state of a helicopter system operating in a chaotic mode is disastrous.

Chaotic oscillations in a helicopter are dangerous as they lead to a loss of control and crashes. Furthermore, oscillations damage equipment and auxiliary systems. For instance, if a blade of a main rotor flips too frequently or its amplitude is too large, it may undergo cracking. In this instance, when chaos is produced, the flipping angles frequently oscillate with large amplitude within $a \in [-14,\ 14]\,\mathrm{rad} = [-802,\ 802]^\circ$ and $b \in [-8,\ 2.4]\ \mathrm{rad} = [458,\ 137]^\circ$ (Fig. 5d), and hence, flipping blades lose performance and control.

Remark 5 The research on the chaotic motion of helicopter systems is important for designing controllers and identifying parameter configurations that avoid instabilities that produce chaos through improper assembly or selection of materials.

4 Bifurcation of helicopter

To test further the adequacy of the helicopter model, we provide a simple analysis of bifurcation obtained from the LE spectra and the double-parameter bifurcation diagram.

The masses of the helicopter's equipment and accessories and their assembled structure will influence the moment of inertia and further impact the hovering dynamics. From the values of the moments of inertia obtained by Tang et al. [25,26], Mahony and Hamel [27], and Kim and Tilbury [28], I_x, I_y, I_z can be taken in the respective ranges of $I_x \in [0.01, 1]$, $I_y \in [0.01, 1]$, $I_z \in [0.01, 1]$. We look at three different configurations:

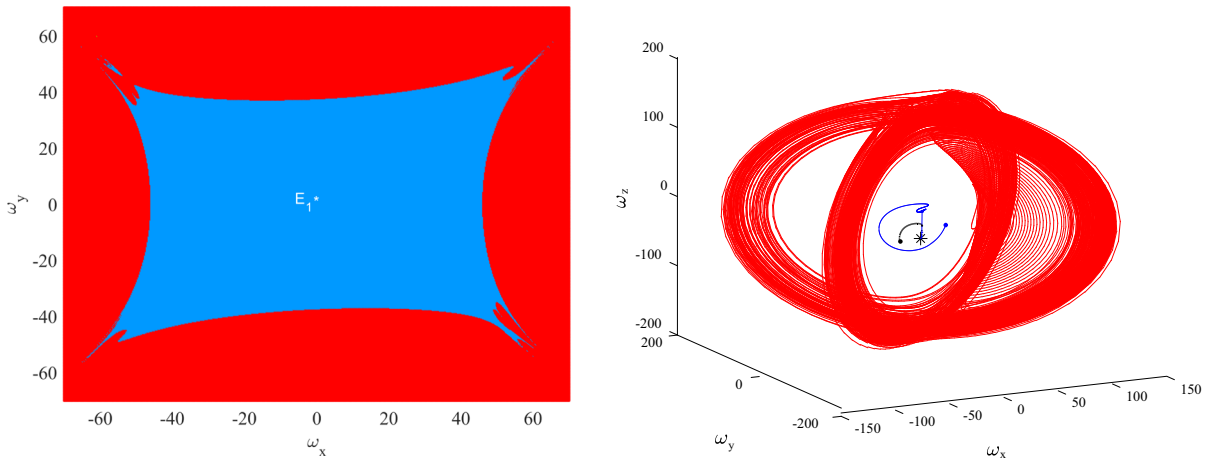

(a) Basins of sink and chaos

(b) Two stable-focus modes and a chaotic mode

Fig. 4 Basin of sink attractor and hidden chaotic attractor for settings $\omega_z = -29.5451,\ a = -0.0892$, b=0.0584. (Color figure online)

(1) Fixing $I_x = 0.29,\ I_y = 0.233$, and varying I_z
We obtained the maximum LE spectrum with respect to I_z (Fig. 6a). The chaotic mode exists in a narrow range, $I_z \in [0.231,\ 0.245]$. If $I_z \in [0.0014,\ 0.018]$, $L_1 = 0$, indicating that the system is in a pseudo-periodic or periodic orbital mode. If I_z is within other intervals, $L_1 < 0$, corresponding to a sink mode.
(2) Fixing $I_x = 0.29,\ I_z = 0.236$ and varying I_y
The chaotic mode exists in a narrow range, $I_y \in [0.01,\ 0.22]$ with $L_1 > 0$ (Fig. 6b); if $I_y \in (0.22,\ 0.236]$, the system is in a pseudo-periodic or periodic orbital mode; otherwise, the system is in a stable state.
(3) Fixing $I_x = 0.29$ and varying I_y and I_z

The two-dimensional LE spectrum features locations of different dynamics over a large area and hence presents a more general overview of the parameter configurations. In Fig. 6c, colors indicate values of the maximum LE; see color bar index. The image is divided into three regions: red indicating chaotic modes for the helicopter system if I_y and I_z fall within this area, and the yellow and green regions indicating pseudo-periodic or periodic orbital modes. If I_y and I_z fall within the blue area, the system operates in a stable state, implying that the configuration of the moments of inertia is reasonable for hovering. To explain clearly the two-dimensional (2D) bifurcation, we illustrate the idea with one point from each colored area. Point $[I_y,\ I_z]^{\mathrm{T}} = [0.239,\ 0.238]^{\mathrm{T}}$ is in the red area with $L_1 = 0.19,\ L_2 = 0$, so the helicopter is in chaotic mode (Fig. 6d1. Point $[I_y,\ I_z]^{\mathrm{T}} = [0.053,\ 0.1]^{\mathrm{T}}$ is in the green area with $L_1 = 0,\ L_2 = 0$, so the system is in pseudo-periodic orbital mode (Fig. 6d2). Point $[I_y,\ I_z]^{\mathrm{T}} = [0.233,\ 0.254]^{\mathrm{T}}$ is in the yellow area with $L_1 = 0,\ L_2 = -0.18$ indicating that the system produces a periodic orbit (Fig. 6d3). Point $[I_y,\ I_z]^{\mathrm{T}} = [0.55,\ 0.5]^{\mathrm{T}}$ is in the blue area with $L_1 = -0.41,\ L_2 = -0.59$, indicating that the system is in a stable mode (Fig. 6d4), which is the normal operating state for a hovering helicopter.

5 Control of the unmanned helicopter

In hovering state, the main thrust was kept for $T_m = mg$ to counteract the gravitational force, and therefore, the main thrust is fixed. In addition, we took $T_t = 4$N to keep the helicopter from rotating around the z axis. When the chaos behavior appears, we have to control the helicopter, otherwise, it will crash. As shown in Fig. 2, normally we have to add the control inputs u_{lon} and u_{lat} to change longitudinal and lateral flapping angle motions a and b and further stabilize the angular velocity ω_x and ω_y. The controlled helicopter in hovering state is written as follows:

$$I_x\dot{\omega}_x = (I_y - I_z)\omega_y\omega_z + (K_\beta + h_m T_m)sb - Q_m sacb - h_t T_t,$$
$$I_y\dot{\omega}_y = (I_z - I_x)\omega_x\omega_z + (K_\beta + h_m T_m)sa$$

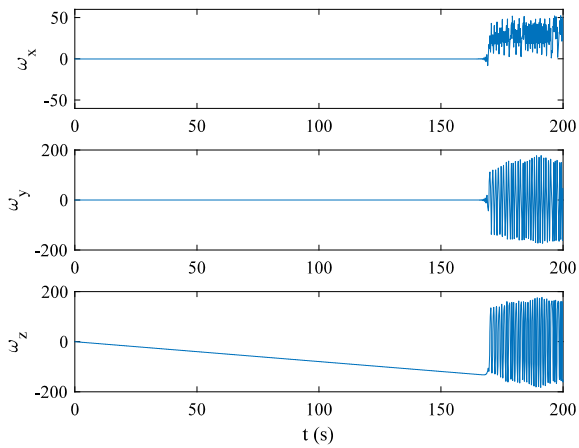

(a) Time responses of ω_x, ω_y and ω_z

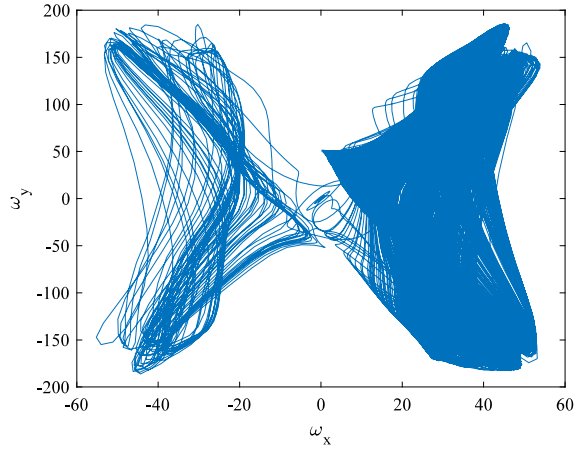

(b) Phase portrait of ω_x-ω_y

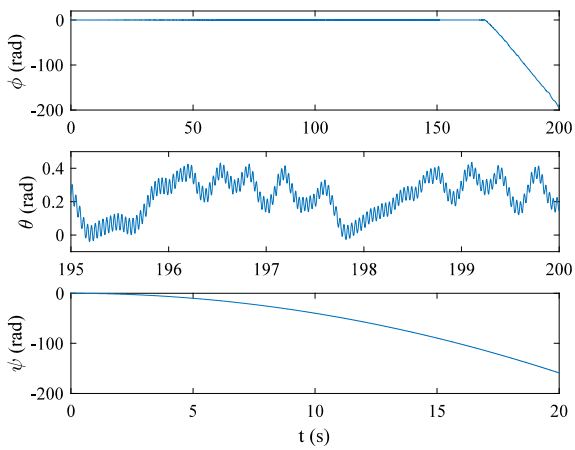

(c) Euler angles

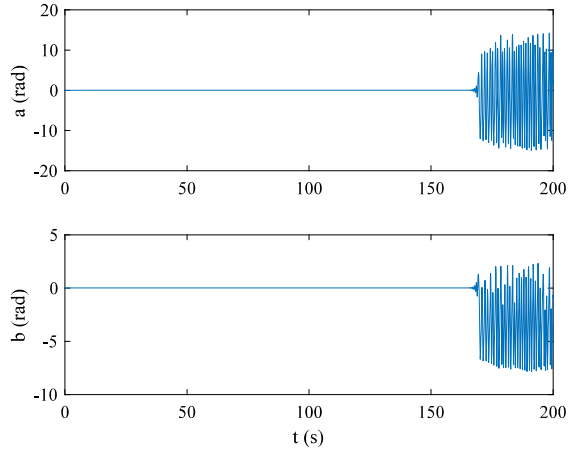

(d) Flipping angles of main rotor

Fig. 5 Chaotic state with initial values starting at origin, and moment of inertia $I_x = 0.29\text{kg m}^2$, $I_y = 0.233\text{kg m}^2$, $I_z = 0.236\text{kg m}^2$

$$
\begin{aligned}
&+Q_m sbca - Q_t,\\
I_z\dot{\omega}_z &= (I_x - I_y)\omega_x\omega_y - Q_m cacb + l_t T_t,\\
\dot{a} &= -\omega_y - 1/\tau a + A_b b + A_{lon}u_{lon},\\
\dot{b} &= -\omega_x - 1/\tau b + B_a a + A_{lat}u_{lat}.
\end{aligned} \tag{16}
$$

where T_t is the third control input serving for the angular velocity ω_z in the control channel of the third sub-equation of Eq. (16). The system is under-actuated, because it has three active inputs to actuate directly. However, it is still a MIMO system. Using the third sub-equation, based on the reference input ω_{zr}, T_t can be designed. Based on the references ω_{xr} and ω_{yr}, using the first and the second sub-equations, flapping angle motions a and b will be the intermediate control laws, which takes the roles of the reference input for the fourth and fifth sub-equations to determine control inputs u_{lon} and u_{lat}. Therefore, this scheme is quite complicated.

When the helicopter angular velocity is in normal situation, it is easy to control it using multiple PIDs, sliding mode controllers, or other controllers. However, when system behavior enters into chaos orbit, the normal control methods will fail even if many controllers are employed, because the dynamics is highly unstable and the change is so fast that the control input cannot follow it. We applied Tereshko control method [20], which only needs a single controller for multi-dimensional system. The controller takes the role of perturbation using as little as energy to counteract or

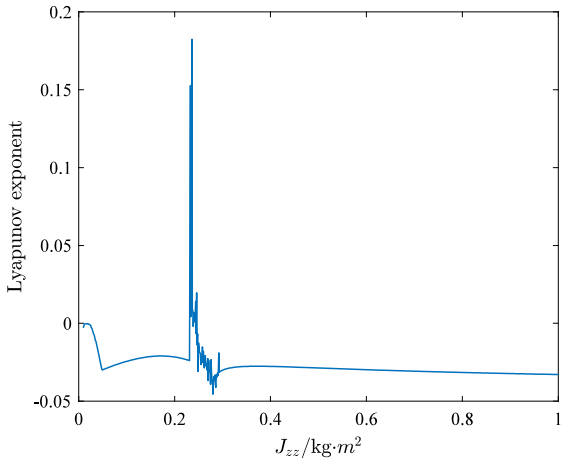

(a) Maximum LE spectrum versus I_z.

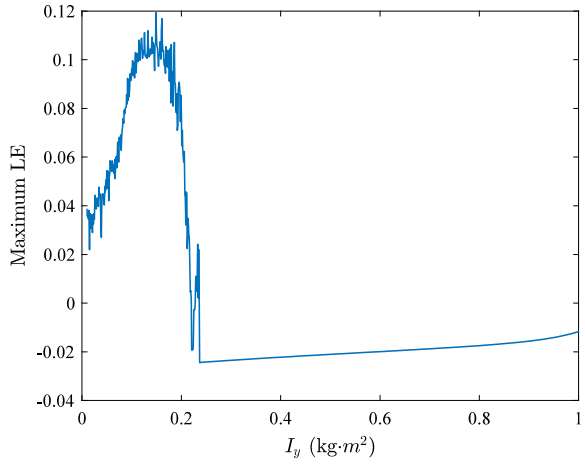

(b) Maximum LE spectrum versus I_y.

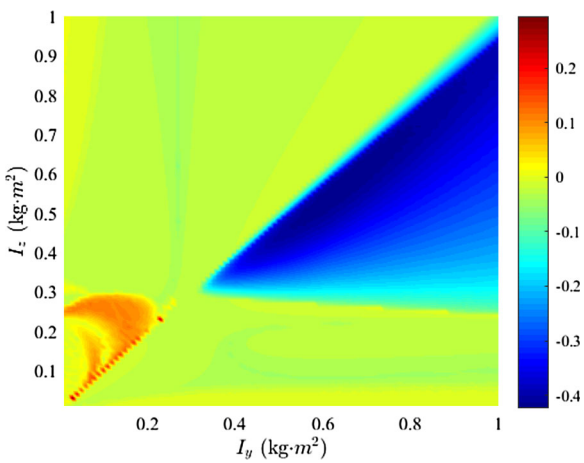

(c) Double-parameter bifurcation diagram

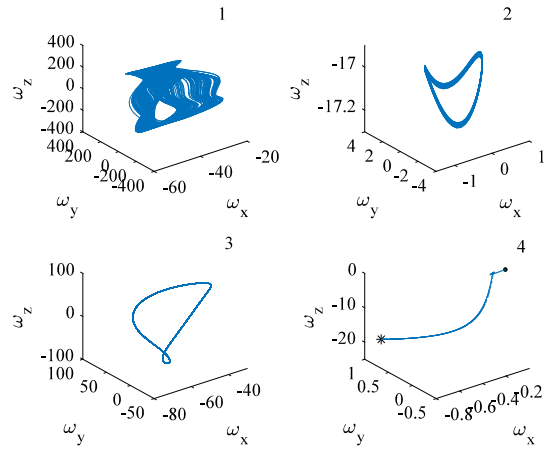

(d) Four different dynamics

Fig. 6 Bifurcation diagrams. (Color figure online)

suppress the energy exchange between dissipation and supplying. The nonlinear feedback control form is as follows

$$u = -k \tanh(\beta \dot{x}). \tag{17}$$

This controller has been designed for a second-order system with $k > 0$ [20]. It has the property that when the velocity $\dot{x}$ is positive, the control input u is negative which stabilizes (destabilizes) the behavior when energy increases (decreases). The control method is quite effective in controlling both SISO and MIMO systems with just one controller added in control channel [20,29]. However, the helicopter is a coupled MIMO system with five sub-equations, and each of which is a first-order equation, which does not fix the requirement of the second-order plant. Hence, we replace $\dot{x}$ with x, and the modified controller is as follows

$$u = -k \tanh(\beta x). \tag{18}$$

This controller takes a nonlinear negative feedback role. Since only one controller is needed, many choices can be taken. The control input can be either u_{lon} or u_{lat} or T_t. If T_t is set as control input, the first and the second sub-equations will be effected for Q_t containing T_t from Eq. (9). This choice still makes the control complicated. Therefore, we may set either u_{lon} or u_{lat} as control input. Let

$$u_{lon} = -k \tanh(\beta a). \tag{19}$$

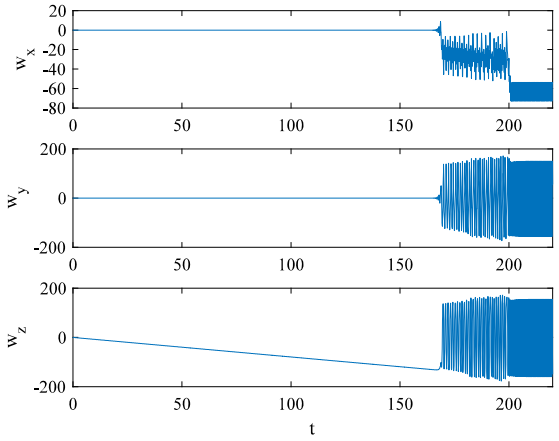

(a) starting at origin, and then entering chaos and then being controlled into periodic orbit

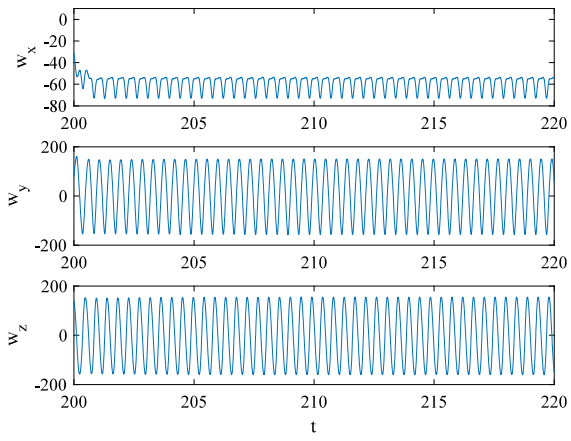

(b) Chaos trajectory being suddenly lead to periodic orbit

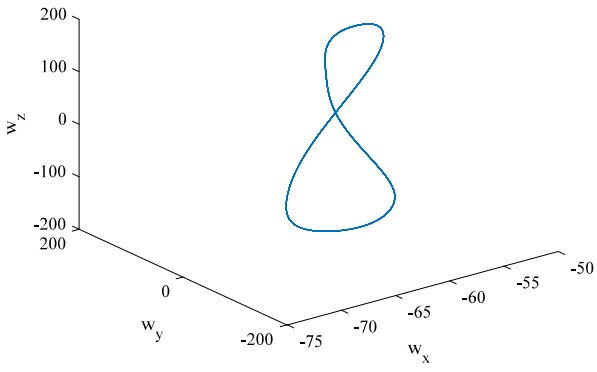

(c) periodic orbit after being controlled

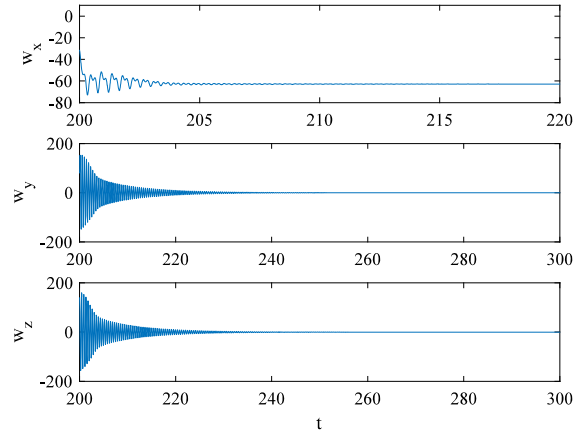

(d) chaotic behavior being stabilized to an equilibrium point

Fig. 7 Control effect, $k = 7$ for (**a**–**c**), $k = 18$ for (**d**)

For instance, taking $k = 7$ and $\beta = 10$, the controller is able to lead the orbit out from the chaotic behavior to periodic orbit. Prior to 200 s, the system is subjected to no control besides fixing $T_m = mg$ and $T_t = 4$N, so when $t = 166$s, chaos emerges (Fig. 7a). When $t = 200$s, the control input (19) takes effect, and then, suddenly the chaotic behavior is suppressed, and periodic orbit appears (Fig. 7a). The times series of periodic trajectory are shown within the time interval $t \in [200,\ 220]$, which clearly demonstrates the effectiveness after control. 3D space observation further confirms the periodic orbit (Fig. 7c).

Taking $k = 18$ and $\beta = 10$, the chaotic behavior is finally convergent to the equilibrium point (Fig. 7d) at

$$E_3 = \left[\omega_x,\ \omega_y,\ \omega_z,\ a,\ b\right]^{\mathrm{T}}_{E_1} = [-62.8409,\ -0.0513,\ -0.3039,\ -0.0308, 6.2964]^{\mathrm{T}},$$

for system (16). This can be verified by substituting E_3 to the left sub-equations of Eq. (16) resulting in zeros. Therefore, this control is effective in driving the angular velocity of the helicopter to the periodic orbit or stabilizing it to equilibrium point.

This perturbation control method has the merits: (1) needing a single controller; (2) no needing the control input computation.

6 Conclusion

The dynamical attitude model of a small-scale unmanned helicopter was built. The dynamics of the system has been analyzed using the parameter values of MIT's small-scale rotorcraft X-Cell 60.

Chaotic behaviors in terms of angular velocity have been identified when initials are selected around a saddle equilibrium point. This confirms that this chaos is self-excited by the saddle point. The chaotic behavior, even little oscillation, is not desired for helicopter, and therefore, it should be investigated. The hidden chaos in a large region, in another word the non-self-excited chaos, also has been observed, which warns that a normal (stable) flight under a perturbation may enter into hidden chaotic region and cause disaster. Through bifurcation analysis, we found that when the distribution of moment of inertia is changed, chaotic behavior also appears. This points out that unsuitable configuration of inertia or shape of the helicopter also are the source of abnormal motion. When the small-scale unmanned helicopter system undergoing excessive oscillations causes unnecessary energy loss and even damage to the motor, its dynamical analysis in terms of the parameter configuration for this open-loop system prior to designing the controller helps in realizing an efficient closed-loop system control and strong decision-making as well as good mission planning. The proposed model and the uncovering of chaotic modes provide a benchmark in the design and control algorithm research of similar helicopters.

Bifurcation analyses with respect to other physical parameters, such as mass, spring constants, tail rotor hub location, air resistance, and damping ratio, have not been conducted. When the given references are Euler angles, how to control the system to the desired orientation subjecting to chaos situation shall be studied. Each impacts the dynamics of a small-sized hovering helicopter. Much work remains and is left as an open research topic.

Acknowledgements This work is supported by the National Natural Science Foundation of China (61873186) and the Natural Science Foundation of Tianjin City (17JCZDJC38300). We thank Richard Haase, Ph.D., from Liwen Bianji, Edanz Group China (www.liwenbianji.cn/ac), for editing the English text of a draft of this manuscript.

Compliance with ethical standards

Conflict of interest The authors declare that they have no conflict of interest.

References

1. Cai, G.W., Chen, B.M., Tong, H.L.: Unmanned Rotorcraft Systems, pp. 14–15. Springer, Berlin (2011)
2. Koo, T., Sastry, S.: Output tracking control design of a helicopter model based on approximate linearization. In: Proceedings of 37th IEEE Conference Decision Control, vol. 4, pp. 3635–3640 (1998)
3. Kendoul, F.: Survey of advances in guidance, navigation, and control of unmanned rotorcraft systems. J. Field Robot **29**(2), 315–378 (2012)
4. Bhandari, S., Colgren, R.: High-order dynamics models of a small UAV helicopter using analytical and parameter identification techniques. J. Am. Helicopter Soc. **60**, 1–10 (2015)
5. Tischler, M.B., Cauffman, M.G.: Frequency-response method for rotorcraft system identification: flight applications to BO 105 coupled rotor/fuselage dynamics. J. Am. Helicopter Soc. **37**, 3–17 (1992)
6. Raptis, I.A., Valavanis, K.P., Moreno, W.A.: A Novel nonlinear backstepping controller design for helicopters using the rotation matrix. IEEE Trans. Control Syst. Technol. **19**, 465–473 (2011)
7. Pan, Y., Song, P., Li, K., Wang, Y., Wang, X.: Attitude dynamics modeling of a small-scale unmanned helicopter. IEEE **88**, 84 (2012)
8. Mettler, B., Tischle, M.B., Kanade, T.: System identification modeling of a small-scale unmanned rotorcraft for flight control design. J. Am. Helicopter Soc. **14**, 50–63 (2002)
9. Mota, S. D. J., Botez, R. M.: New identification method based on neural network for helicopters from flight test data. In: AIAA Atmosphere Flight Mechanics Conference, 092407, pp. 1–31 (2009)
10. Qi, G., Hu, J.: Force analysis and energy operation of chaotic system of permanent-magnet synchronous motor. Int. J. Bifurc. Chaos **27**, 1750216 (2017)
11. Qi, G.: Energy cycle of brushless DC motor chaotic system. Appl. Math. Model. **51**, 686–697 (2017)
12. Qi, G., Liang, X.: Mechanical analysis of Qi four-wing chaotic system. Nonlinear Dyn. **86**, 1095–1106 (2016)
13. Qi, G., Liang, X.: Force analysis of Qi chaotic system. Int. J. Bifurc. Chaos **26**, 1650237 (2016)
14. Hemati, N.: Strange attractors in brushless DC motors. IEEE Trans. Circuits Syst. I Fundam. Theory Appl. **41**(1), 40–45 (1994)
15. Pikovskii, A.S., Rabinovich, M.I., Trakhtengerts, V.Y.: Onset of stochasticity in decay confinement of parametric instability. Sov. Phys. JETP **47**, 715–19 (1978)
16. Yang, Y., Qi, G.: Mechanical analysis and bound of plasma chaotic system. Chaos Solitons Fractals **108**, 187–195 (2018)
17. Yang, Y., Qi, G.: Comparing mechanical analysis with generalized-competitive-mode analysis for the plasma chaotic system. Phys. Lett. A **383**, 318–327 (2019)

18. Qi, G.: Modelings and mechanism analysis underlying both the 4D Euler equations and Hamiltonian conservative chaotic systems. Nonlinear Dyn. **95**, 2063–2077 (2019)
19. Xu, W., Li, Q.: Chemical chaotic schemes derived from NSG system. Chaos Solitons Fracals **15**, 663–671 (2003)
20. Tereshko, V.: Control and identification of chaotic systems by altering their energy. Chaos Solitons Fractals **40**(5), 2430–2446 (2009)
21. Gavrilets, V., Mettler, B., Feron, E.: Dynamical Model for a Miniature Aerobatic Helicopter, pp. 1–22. Massachussetts Institute of Technology, Boston (2001)
22. Liang, X., Qi, G.: Mechanical analysis of Chen chaotic system. Chaos Solitons Fractals **98**, 173–177 (2017)
23. Dudkowski, D., Jafari, S., Kapitaniak, T., Kuznetsov, N.V., Leonov, G.A., Prasad, A.: Hidden attractors in dynamical systems. Phys. Rep. **637**(3), 1–50 (2016)
24. Zhang, S., Zeng, Y., Li, Z., et al.: A novel simple no-equilibrium chaotic system with complex hidden dynamics. Int. J. Dyn. Control **6**, 1465–1476 (2018)
25. Tang, S., Zheng, Z., Qian, S., Zhang, X.: Nonlinear system identification of a small-scale unmanned helicopter. Control Eng. Pract. **25**, 1–15 (2014)
26. Tang, S., Yang, Q., Qian, S., et al.: Height and attitude active disturbance rejection controller design of a small-scale helicopter. Sci. China Inf. Sci. **58**(3), 1–17 (2015)
27. Mahony, R., Hamel, T.: Robust trajectory tracking for a scale model autonomous helicopter. Int. J. Robust Nonlinear **14**, 1035–1059 (2004)
28. Kim, S., Tilbury, D.: Mathematical modeling and experimental identification of an unmanned helicopter robot with flybar dynamics. J. Robot. Syst. **21**, 95–116 (2004)
29. Avanço, R.H., Tusset, A.M., Balthazar, J.M.: Nabarrete1 A, Navarro H A, On nonlinear dynamics behavior of an electromechanical pendulum excited by a nonideal motor and a chaos control taking into account parametric errors. J. Braz. Soc. Mech. **40**(23), 1–17 (2018)